Electronic transport properties of PbTe and $AgPb_mSbTe_{2+m}$ systems

D. I. Bilc
Condensed Matter Sciences Division, Oak Ridge National Laboratory, Oak Ridge, Tennessee 37831, USA and Department of Physics and Astronomy, University of Tennessee, Knoxville, Tennessee 37996, USA

S. D. Mahanti
Department of Physics and Astronomy, Michigan State University, East Lansing, Michigan 48824, USA

M. G. Kanatzidis
Department of Chemistry, Michigan State University, East Lansing, Michigan 48824, USA

(Received 27 September 2005; revised manuscript received 27 April 2006; published 8 September 2006)

Transport calculations using the Boltzmann equation within energy-dependent relaxation time approximations were performed for PbTe and $AgPb_mSbTe_{2+m}$ (LAST-m) systems. We have used both the nonparabolic Kane model for the energy dispersion and the energy dispersion given by *ab initio* electronic structure calculations. For PbTe we find that the temperature dependence of the density of states effective mass m_d is very important in order to have good agreement with experiment for electrical conductivity σ and thermopower S. Transport calculations in n-type PbTe using the energy dispersion given by the *ab initio* electronic structure results in overestimation of σ and underestimation of S because the temperature dependence of m_d cannot be incorporated in the calculation of the chemical potential. Transport calculations in n-type LAST-m systems using the nonparabolic Kane model for the energy dispersion show a small enhancement of the power factor (σS^2) in 0–500 K temperature range relative to PbTe. The observed large ZT values of the LAST-12 and LAST-18 systems are a combination of a small enhancement of the power factor and a strong reduction in the thermal conductivity due to the formation of Ag-Sb microstructures.

DOI: 10.1103/PhysRevB.74.125202 PACS number(s): 71.15.Mb, 71.20.−b, 71.20.Nr, 72.10.−d

I. INTRODUCTION

A new class of quaternary thermoelectric compounds $AgPb_mSbTe_{2+m}$, denoted as LAST-m, has attracted considerable attention during the last two years because of their large figure of merit ZT ($ZT\sim1.2$ for LAST-12 and ~1.8 for LAST-18 at 800 K).[1] The dimensionless figure of merit ZT describes the thermoelectric performance of a material and is defined as $ZT=\sigma S^2T/\kappa$, where σ is the electrical conductivity, S is the thermopower, κ is the thermal conductivity, and T is the absolute temperature. These compounds form in the rock-salt structure ($Fm\bar{3}m$ symmetry) similar to the binary PbTe, where Ag and Sb occupy Pb sites. One expects that by replacing two divalent Pb atoms by a monovalent Ag atom and a trivalent Sb atom, one maintains the charge compensation and the resulting system will be a narrow band gap semiconductor. By controlling the Ag and Sb concentration and their spatial ordering one can manipulate the electronic structure and consequently their transport properties. There is clear experimental evidence from single crystal x-ray diffraction and high resolution electron microscopy studies that LAST-m systems are not simple solid solutions between $AgSbTe_2$ and PbTe phases.[2] Rather, they exhibit microscopic inhomogeneities rich in Ag-Sb embedded into a PbTe matrix.

Our recent electronic structure calculations for different microstructural arrangements of Ag and Sb in LAST-m systems have revealed that these have an enhanced density of states (DOS) near the gap as compared to the bulk PbTe due to the appearance of distinct resonant states.[3] It has been suggested that resonant structures in the DOS near the chemical potential, created by quantum size effects,[4–6] superlattice engineering,[7] or chemical means,[8–10] are desirable features because they could enhance the thermoelectric figure of merit ZT. Therefore, it is important to know how these features in the DOS affect the electronic transport properties such as electrical conductivity σ and thermopower S, the two quantities which define the power factor PF (PF$=\sigma S^2$). Also, it is important to understand why LAST-m systems show larger ZT than PbTe, whether due to higher PF or due to reduced thermal conductivity κ.

In order to answer the above questions and also to see how well theory can describe quantitatively different transport coefficients, we have performed finite temperature electronic transport calculations in n-type PbTe and LAST-m systems. These calculations were performed using Boltzmann transport equations within the energy-dependent relaxation time approximation and the nonparabolic Kane model for the energy dispersion $\epsilon_{\vec{k}}$ vs $\vec{k}$.[11] Also, the energy dispersion given by *ab initio* electronic structure calculations has been used in some of the calculations. We have considered the temperature dependence of the density of states effective mass m_d[12] and the band gap E_g between the valence band maximum and conduction band minimum.[13] These were taken from the experiment. Ravich *et al.* have taken into account the temperature dependence of m_d through the temperature dependence of E_g.[14,15] This is only valid for small variations of m_d near the band edge. Furthermore, the experimental results in PbTe show that E_g increases with temperature for $T\leq 400$ K and is constant for $T>400$ K,[13] whereas m_d increases with T even for $T>400$ K.[12]

Several earlier attempts to incorporate the energy and temperature dependence (through band gap and effective

mass) of different scattering mechanisms in the calculation of transport properties of PbTe have been made.[14–17] Ravich *et al.* have considered polar optical phonon, acoustic phonon, and impurity scattering as the dominant scattering mechanisms. Zayachuk[16] and Freik *et al.*[17] have pointed out that deformation potential coupling with optical phonons is also important in certain temperature ranges. In this paper we take into account all the scattering mechanisms over a broad temperature range (0–950 K), in addition to taking into account the temperature dependence of band gap E_g and density of states effective mass m_d. Our focus is on the high temperature end because of the current interest in high-T thermoelectrics.

II. TRANSPORT COEFFICIENTS USING THE BOLTZMANN EQUATION

A standard method to deal with charge and energy transport is to use the Boltzmann transport equation.[18] In the relaxation time approximation, the different transport coefficient tensors, $\overleftrightarrow{\sigma}$ (electrical conductivity), $\overleftrightarrow{S}$ (thermoelectric coefficient or thermopower), and $\overleftrightarrow{\kappa}_0$ (electronic thermal conductivity at zero electric field $\vec{E}$ rather than at zero current $\vec{J}$) are given by

$$\overleftrightarrow{\sigma} = \frac{e^2}{V}\sum_{\vec{k}}\left(-\frac{\partial f_{\vec{k}}}{\partial \epsilon_{\vec{k}}}\right)\tau_{\vec{k}}\vec{v}_{\vec{k}}\vec{v}_{\vec{k}}, \tag{1}$$

$$\overleftrightarrow{S} = (\overleftrightarrow{\sigma})^{-1}\overleftrightarrow{A}, \tag{2}$$

$$\overleftrightarrow{\kappa}_0 = \frac{1}{VT^2}\sum_{\vec{k}}\left(-\frac{\partial f_{\vec{k}}}{\partial \epsilon_{\vec{k}}}\right)(\epsilon_{\vec{k}}-\mu)^2\vec{v}_{\vec{k}}\vec{v}_{\vec{k}}\tau_{\vec{k}}, \tag{3}$$

where $\overleftrightarrow{A}$ is given by

$$\overleftrightarrow{A} = \frac{e}{VT}\sum_{\vec{k}}\left(-\frac{\partial f_{\vec{k}}}{\partial \epsilon_{\vec{k}}}\right)(\epsilon_{\vec{k}}-\mu)\tau_{\vec{k}}\vec{v}_{\vec{k}}\vec{v}_{\vec{k}}. \tag{4}$$

In Eqs. (1), (3), and (4), e is electronic charge, V is the volume in real space, $\tau_{\vec{k}}$ is the relaxation time, $\vec{v}_{\vec{k}}$ is the velocity of charge carriers, and $f_{\vec{k}}$ is the equilibrium Fermi distribution function at temperature T and chemical potential μ.

III. NONPARABOLIC KANE MODEL FOR ENERGY DISPERSION

In this section we will discuss a simple but highly successful model for the band structure of PbTe. In narrow band-gap semiconductors (i.e., lead chalcogenides) the energy region of interest of an electron as measured from the band edge is comparable to the band gap E_g. Because of this, the dependence of the energy on crystal momentum is nonquadratic and the effective masses are functions of the energy. The nonparabolic Kane model was introduced to describe the deviations from the quadratic dependence of energy on the crystal momentum $\vec{k}$.[11] In this model, the longitudinal effective mass m_l and the transverse effective mass m_t depend only on the interaction between the lowest conduction band and the highest valence band and the contributions of other bands are assumed to be small. In Fig. 1 the band structure of PbTe obtained by *ab initio* electronic structure calculations is shown. The conduction band minimum and the valence band maximum in PbTe occur at the $L[1/2,1/2,1/2]$ point; coordinates are expressed in units of the primitive face-centered-cubic reciprocal lattice vectors. The longitudinal effective mass m_l is defined along the $L\Gamma$ direction in the Brillouin zone, whereas the transverse effective mass m_t is defined along the perpendicular direction to $L\Gamma$. For the simple parabolic model the energy dispersion can be expressed as

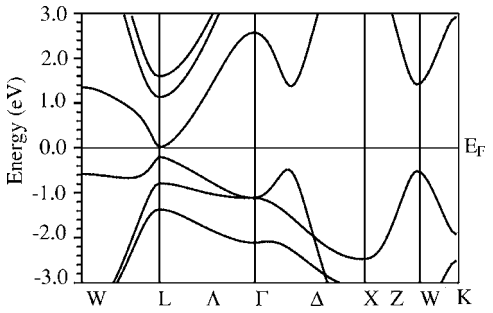

FIG. 1. Band structure of PbTe in face centered cubic Brillouin zone.

$$\epsilon_{\vec{k}} = \frac{\hbar^2}{2}\left(\frac{2k_t^2}{m_t}+\frac{k_l^2}{m_l}\right), \tag{5}$$

where $\epsilon_{\vec{k}}$ is the energy, and k_l and k_t are the magnitudes of the longitudinal and transverse components of $\vec{k}$ (measured from the L point). In the Kane model the energy dispersion is given by

$$\epsilon_{\vec{k}}\left(1+\frac{\epsilon_{\vec{k}}}{E_g}\right) = \frac{\hbar^2}{2}\left(\frac{2k_t^2}{m_t}+\frac{k_l^2}{m_l}\right). \tag{6}$$

In this model the effective masses and the mass anisotropy coefficient of electrons and holes are equal. The constant energy surfaces are ellipsoids, and m_l and m_t have the same energy dependence.

IV. TRANSPORT COEFFICIENTS IN THE KANE MODEL

In order to calculate the transport coefficients we have to compute different quantities appearing in Eqs. (1), (3), and (4), which include the carrier velocity $\vec{v}_{\vec{k}}$ and the relaxation time $\tau_{\vec{k}}$. For this, $\vec{v}_{\vec{k}}$ and $\tau_{\vec{k}}$ for different scattering mechanisms have to be evaluated within the Kane model. The calculations of the relaxation times were carried out by Ravich *et al.*,[14] and these expressions are given in Sec. V for completeness.

PbTe and the LAST-m systems on average have cubic symmetry. Therefore, the components $\sigma_{\mu\nu}$ and $S_{\mu\nu}$ of the electrical conductivity and thermopower tensors can be expressed as

$$\sigma_{\mu\nu} = \delta_{\mu\nu}\sigma, \tag{7}$$

$$S_{\mu\nu} = \delta_{\mu\nu} S, \tag{8}$$

where σ and S are related to the trace of $\overleftrightarrow{\sigma}$ and $\overleftrightarrow{S}$ tensors and are given by

$$\sigma = \frac{1}{3} \mathrm{Tr}\, \overleftrightarrow{\sigma}, \tag{9}$$

$$S = \frac{1}{3} \mathrm{Tr}\, \overleftrightarrow{S}. \tag{10}$$

$\mathrm{Tr}\, \overleftrightarrow{\sigma}$ and $\mathrm{Tr}\, \overleftrightarrow{S}$ only depend on $\vec{v}_{\vec{k}}^2$. The detailed expressions for thermopower S_{xx}, electrical conductivity σ_{xx} along the x axis, and the carrier concentration n are given in the Appendix [Eqs. (A11), (A14), and (A16)]. In the limit of constant relaxation time $\tau_\epsilon = \tau_0$, independent of energy ϵ, the expressions for thermopower, electrical conductivity, and concentration have a simplified form,

$$S_{xx} = \frac{k_B}{e}\left(\frac{{}^1L_{-1}^{3/2}(\mu, E_g)}{{}^0L_{-1}^{3/2}(\mu, E_g)} - \mu\right), \tag{11}$$

$$\sigma_{xx} = \frac{2}{3}\gamma e^2 \frac{(2m_d')^{1/2}\tau_0}{\pi^2\hbar^3}[{}^0L_{-1}^{3/2}(\mu, E_g)], \tag{12}$$

$$n = \frac{1}{3}\gamma \frac{(2m_d')^{3/2}}{\pi^2\hbar^3}[{}^0L_0^{3/2}(\mu, E_g)], \tag{13}$$

where k_B is the Boltzmann constant, γ is the band degeneracy, m_d' is related to the density of states effective mass m_d [Eq. (A17)], and ${}^nL_l^m(\mu, E_g)$ are the generalized Fermi integrals given by

$${}^nL_l^m(\mu, E_g) = \int_0^\infty \left(-\frac{\partial f}{\partial \epsilon}\right)(\epsilon)^n \left[\epsilon\left(1 + \frac{\epsilon}{E_g}\right)\right]^m \left(1 + \frac{2\epsilon}{E_g}\right)^l d\epsilon. \tag{14}$$

Note that in this limit S_{xx} is independent of the relaxation time, and systems with large differences in σ_{xx} caused by different τ_0 can have the same S_{xx}. This approximation is rather poor for PbTe and related materials.

V. RELAXATION TIMES IN THE KANE MODEL

Different scattering mechanisms of charge carriers in lead chalcogenides have been intensively studied in many papers.[11,14–17] It is found that the dominant scattering mechanisms are by point defects and by thermal phonons, and their relative contributions to the scattering processes are summarized below.

At low temperatures (liquid helium), charge carriers are scattered mostly by charged vacancies. At low densities $n \leq 5 \times 10^{18}$ cm^{-3}, scattering by Coulomb potential of the vacancies dominates, whereas for high carrier densities $n \geq 10^{19}$ cm^{-3}, the Coulomb potential gets screened out and scattering by the short range potential of vacancies dominates. As the temperature increases, the relative importance of the charged vacancies decreases and scattering by thermal phonons increases. For temperatures above 300 K, scattering by acoustic phonons and optical phonons (both polar and deformation potential) contribute mostly to the relaxation time.

The expressions for the dominant contributions to the relaxation time within the Kane model are available in the literature.[14,16,17] Therefore we give here only the final expressions for different scattering mechanisms, discuss the fundamental parameters involved, and analyze their relative significance for PbTe and the related LAST-m systems.

(i) Deformation potential of acoustic phonons (τ_a)

$$\tau_a = \frac{\tau_{0,a}(T)\left(\epsilon + \frac{\epsilon^2}{E_g}\right)^{-1/2}}{\left(1 + 2\frac{\epsilon}{E_g}\right)[(1-A)^2 - B]}, \tag{15}$$

$$A = \frac{\frac{\epsilon}{E_g}(1 - K_a)}{\left(1 + 2\frac{\epsilon}{E_g}\right)}, \tag{16}$$

$$B = \frac{8\frac{\epsilon}{E_g}\left(1 + \frac{\epsilon}{E_g}\right)K_a}{3\left(1 + 2\frac{\epsilon}{E_g}\right)^2}, \tag{17}$$

$$\tau_{0,a}(T) = \frac{2\pi\hbar^4 C_l}{E_{ac}^2 k_B T (2m_{d0})^{3/2}}, \tag{18}$$

where E_{ac} is the acoustic deformation potential coupling constant for the conduction band, C_l is a combination of elastic constants, K_a is the ratio of the acoustic deformation potential coupling constants for the valence and conduction bands $K_a = E_{av}/E_{ac}$, with the values $K_a = 1$ for n-type PbTe and $K_a = 1.5$ for p-type PbTe, and m_{d0} is the density of states effective mass for a single ellipsoid ($\gamma = 1$).

(ii) Deformation potential of optical phonons (τ_o),

$$\tau_o = \frac{\tau_{0,o}(T)\left(\epsilon + \frac{\epsilon^2}{E_g}\right)^{-1/2}}{\left(1 + 2\frac{\epsilon}{E_g}\right)[(1-A)^2 - B]}, \tag{19}$$

$$A = \frac{\frac{\epsilon}{E_g}(1 - K_o)}{\left(1 + 2\frac{\epsilon}{E_g}\right)}, \tag{20}$$

$$B = \frac{8\frac{\epsilon}{E_g}\left(1 + \frac{\epsilon}{E_g}\right)K_o}{3\left(1 + 2\frac{\epsilon}{E_g}\right)^2}, \tag{21}$$

$$\tau_{0,o}(T) = \frac{2\hbar^2 a^2 \rho (\hbar\omega_0)^2}{\pi E_{oc}^2 k_B T (2m_{d0})^{3/2}}, \tag{22}$$

where a is lattice constant, ρ is the density, ω_0 is the frequency of the optical phonons, K_o is the ratio of the optical deformation potential coupling constants for valence and conduction bands, and $K_o = E_{ov}/E_{oc}$. K_o and K_a are assumed to be the same.

(iii) Polar scattering by optical phonons (τ_{po}),

$$\tau_{po} = \frac{\hbar^2 \left(\epsilon + \frac{\epsilon^2}{E_g}\right)^{1/2} F^{-1}}{e^2 (2m_{d0})^{(1/2)} k_B T (\varepsilon_\infty^{-1} - \varepsilon_0^{-1}) \left(1 + 2\frac{\epsilon}{E_g}\right)}, \tag{23}$$

$$F = 1 - \delta \ln(1 + \delta^{-1}) - \frac{2\frac{\epsilon}{E_g}\left(1 + \frac{\epsilon}{E_g}\right)}{\left(1 + 2\frac{\epsilon}{E_g}\right)^2} \times [1 - 2\delta + 2\delta^2 \ln(1 + \delta^{-1})], \tag{24}$$

$$\delta = (2kr_0)^{-2}, \tag{25}$$

where ε_0 and ε_∞ are the static and high frequency permittivities, k is the carrier wave vector, and r_0 is the screening length of the optical phonons. The parameters k and r_0 are given by

$$k^2 = \frac{2m_{d0}\left(\epsilon + \frac{\epsilon^2}{E_g}\right)}{\hbar^2}, \tag{26}$$

$$r_0^{-2} = \frac{2^{5/2} e^2 m_d^{3/2}}{\pi \hbar^3 \varepsilon_\infty} ({}^0L_1^{1/2}). \tag{27}$$

(iv) Short range deformation potential of vacancies (τ_v),

$$\tau_v = \frac{\tau_{0,v}(T)\left(\epsilon + \frac{\epsilon^2}{E_g}\right)^{-1/2}}{\left(1 + 2\frac{\epsilon}{E_g}\right)[(1 - A)^2 - B]}, \tag{28}$$

$$A = \frac{\frac{\epsilon}{E_g}(1 - K_v)}{\left(1 + 2\frac{\epsilon}{E_g}\right)}, \tag{29}$$

$$B = \frac{8\frac{\epsilon}{E_g}\left(1 + \frac{\epsilon}{E_g}\right)K_v}{3\left(1 + 2\frac{\epsilon}{E_g}\right)^2}, \tag{30}$$

TABLE I. Parameters used to calculate the relaxation times for PbTe and LAST-m systems at 300 K.[16]

Parameter	Unit of measurement	Value
m_l/m		0.24
ε_0		400
ε_∞		32.6
C_l	N/m^2	0.71×10^{11}
$\hbar\omega_0$	eV	0.0136
a	Å	6.461
ρ	g/cm^3	8.24
Z		0.14
E_{ac}	eV	15
E_{oc}	eV	26
U_{vc}	ergs cm^3	3×10^{-34}
K_a,K_o, K_v for n type		1.0
K_a, K_o, K_v for p type		1.5

$$\tau_{0,v}(T) = \frac{\pi\hbar^4}{U_{vc}^2 m_{d0} (2m_{d0})^{1/2} N_v}, \tag{31}$$

where N_v is the vacancy density, and K_v is the ratio of the short range deformation potential coupling constants of vacancies for valence and conduction bands, $K_v = U_{vv}/U_{vc}$, which are taken to be the same as for acoustic phonons, K_a.

(v) Coulomb potential of vacancies (τ_C),

$$\tau_C = \frac{\varepsilon_0^2 (2m_{d0})^{1/2}\left(\epsilon + \frac{\epsilon^2}{E_g}\right)^{3/2}}{\pi (Ze^2)^2 N_v [\ln(1 + \xi) - \xi/(1 + \xi)]\left(1 + 2\frac{\epsilon}{E_g}\right)}, \tag{32}$$

$$\xi = (2kr_v)^2, \tag{33}$$

where Ze is the vacancy charge, and r_v is the screening radius of the vacancy potential given by

$$r_v^{-2} = \frac{4\pi e^2}{\varepsilon_0} D(\mu), \tag{34}$$

$$D(\mu) = \frac{2^{1/2} (m_{d0})^{3/2}}{\pi^2 \hbar^3}\left(\mu + \frac{\mu^2}{E_g}\right)^{1/2}\left(1 + 2\frac{\mu}{E_g}\right), \tag{35}$$

$D(\mu)$ being the density of states at the chemical potential, μ.

The total scattering relaxation time τ_ϵ is expressed as

$$\frac{1}{\tau_\epsilon} = \frac{1}{\tau_a} + \frac{1}{\tau_o} + \frac{1}{\tau_{po}} + \frac{1}{\tau_v} + \frac{1}{\tau_C}. \tag{36}$$

The parameters used to calculate the relaxation times were taken from Ref. 16 and they are given in Table I. We find that only the first three terms in the above sum make significant contributions at temperatures above 300 K. The values of the relaxation times at room temperature in the 1–200 meV energy range are $\tau_a = 0.15 - 2.9 \times 10^{-12}$ s, $\tau_o = 0.18 - 2.0 \times 10^{-12}$ s, $\tau_{po} = 0.1 - 0.19 \times 10^{-12}$ s, $\tau_v = 2.4 - 44.7 \times 10^{-12}$ s,

and $\tau_C = 5.2 - 1216.0 \times 10^{-12}$ s. τ_v and τ_C are orders of magnitudes larger than τ_a, τ_o, and τ_{po}.

Experimentally one finds E_g and m_d to be temperature dependent.[12,13] This comes from strong electron-phonon coupling. In our transport calculations we have incorporated the T-dependent E_g and m_d using the experimental data. As discussed later in detail, we find that the temperature dependence of m_d is very important in order to have good agreement with measured values of the transport coefficients. Experimentally it is found that E_g increases linearly with temperature for $T \leq 400$ K and above 400 K, it remains constant.[13] The temperature dependence of $E_g(T)$ is given by

$$E_g = 0.19 + (0.42 \times 10^{-3})T \quad \text{for } T \leq 400 \text{ K}, \tag{37}$$

$$E_g = 0.358, \quad \text{for } T > 400 \text{ K}. \tag{38}$$

The temperature dependence of m_d [see Eq. (A19)] comes primarily through the T-dependence of the transverse effective mass m_t, which is also taken from the experiment[12]

$$\frac{m_t}{m} = 0.024\,59 + (8.659\,341 \times 10^{-5})T, \tag{39}$$

where m is the bare electron mass.

In *ab initio* calculations of transport coefficients using *ab initio* band structure results, one has to carry out summations over all occupied bands. In order to calculate the concentration n, the electrical conductivity σ_{xx}, and thermopower S_{xx}, the sums over $\vec{k}$ have to be taken over different bands. Also, instead of using the equation $\vec{v}(n,\vec{k}) = (1/\hbar)\partial\epsilon(n,\vec{k})/\partial\vec{k}$ for the velocity of an electron in state $n\vec{k}$, we calculate $\vec{v}(n,\vec{k})$ using the momentum matrix elements $\vec{p}(n,\vec{k})$

$$\vec{v}(n,\vec{k}) = \frac{1}{m}\langle p(n,k)\rangle = \frac{1}{m}\langle \psi(n,\vec{k})|\hat{\vec{p}}|\psi(n,\vec{k})\rangle, \tag{40}$$

which are available in the optical properties package of the WIEN2K program.[19] The calculation of relaxation time and its energy dependence using the *ab initio* electronic structure is extremely difficult and will not be attempted here. Instead we will use the energy-dependent relaxation time obtained within the Kane model.

VI. RESULTS AND DISCUSSION

A. PbTe using the Kane model

In order to calculate electrical conductivity σ_{xx} and thermopower S_{xx} for a given concentration n at different temperatures, one has to solve for the chemical potential μ at a give n and T and use this value in the calculation of σ_{xx} and S_{xx}. We use the MATHEMATICA program to solve this problem.

As mentioned in Sec. V, we have taken into account the temperature dependence of E_g and m_d given in Eqs. (37)–(39). At high concentrations, $n \sim 10^{19}$ cm^{-3}, which are required for a good thermoelectric, the n- or p-type PbTe can be described using a single band model since at these concentrations, contributions to transport come primarily from one type of carrier. Here we give the results for the n-type PbTe.

At concentration $n = 5 \times 10^{19}$ cm^{-3}, if we use the strengths of the coupling constants $E_{ac} = 15$ eV and $E_{oc} = 26$ eV as given in Ref. 16 we find that the theoretical value of σ is smaller than experiment [Fig. 2(a)]. The magnitude of the thermopower is, however, slightly higher for $T < 550$K and lower for $T > 550$ K [Fig. 2(c)]. The net effect is a good fit to the power factor PF$=\sigma S^2$ below 400 K [Fig. 2(e)]. The theoretical power factor is considerably smaller than experiment for $T > 400$ K. Thus we are overestimating the strength of the scattering. If we reduce E_{oc} to 15 eV$=E_{ac}$, we find a much better fit to σ over the temperature range 300–950 K [Fig. 2(b)]. Thermopower values are also closer to experiment at higher temperatures [Fig. 2(d)]. The resulting power factor is in better agreement with experiment for $T > 600$ K [Fig. 2(f)]. Because of our interest in the high temperature region, we will use the lower value of E_{oc} in our further analysis.

It is interesting to explore how significant are the temperature dependences of E_g and m_d in the entire temperature range, a study which has not been done carefully in the earlier theoretical calculations.[14–17] For this we calculate σ, S, and the power factor $S^2\sigma$ for a constant m_d using the values $m_l = 0.24m$ and $m_t = 0.024m$. The results for both sets of deformation potential coupling constants are given in Fig. 3. For constant m_d, the electrical conductivity is overestimated whereas the thermopower is underestimated. The temperature dependence of thermopower is not well described; therefore, the inclusion of temperature dependence of m_d is very important to have a good agreement with experimental values of electrical conductivity and thermopower. It is also important to note that one can have fortuitous good agreement for the power factor as shown in Fig. 3(e), even when σ and S are not very well reproduced individually. This further suggests that to understand correctly the temperature dependence of the power factor in PbTe systems, temperature dependence of the electrical conductivity and thermopower have to be studied separately.

We have also considered the case where the energy gap E_g increases linearly with the temperature in the whole 0–950 K temperature range [instead of Eqs. (37) and (38)]. The results for the electrical conductivity and thermopower are given in Fig. 4. We can see that temperature dependence E_g is not crucial for good agreement with experiment at this high concentration, but it is important at low concentrations when carriers from the valence band can be excited into the conduction band across the band gap. For this case a two-band model (conduction and valence) has to be employed to calculate the transport coefficients correctly.

To see whether the good agreement between theoretical values of σ, S, and $S^2\sigma$ and experiment obtained with parameter values $E_{ac} = 15$ eV and $E_{oc} = 15$ eV (values chosen to match the value of σ at 300 K for the concentration $n = 5 \times 10^{19}$ cm^{-3}) persists at different concentrations, we have calculated these quantities at two other concentrations: $n = 2.4 \times 10^{19}$ cm^{-3} and $n = 1 \times 10^{20}$ cm^{-3}. The results are shown in Fig. 5. For $n = 2.4 \times 10^{19}$ cm^{-3}, the room temperature electrical conductivity is slightly underestimated, whereas for $n = 1 \times 10^{20}$ cm^{-3} this value is slightly overesti-

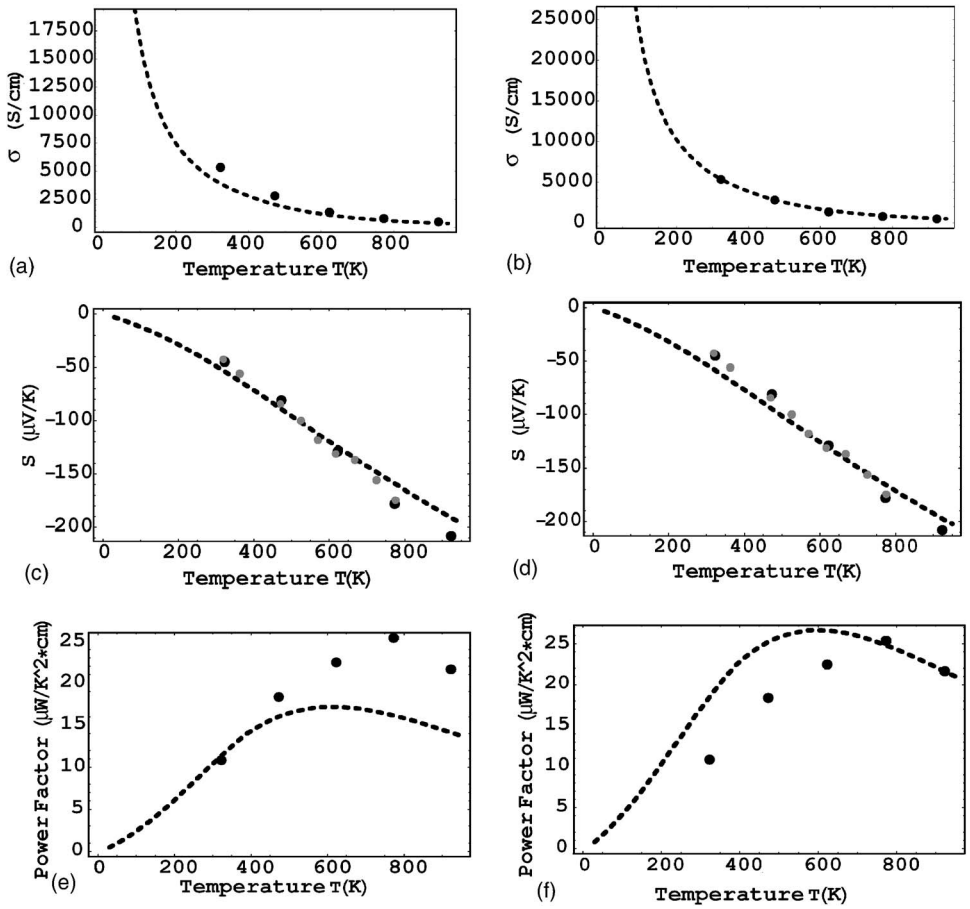

FIG. 2. Temperature dependence of (a) electrical conductivity, (c) thermopower, and (e) power factor for n-type PbTe at concentration $n=5\times10^{19}$ cm^{-3} obtained using $E_{ac}=15$ eV and $E_{oc}=26$ eV values of the deformation potential coupling constants. Temperature dependence of (b) electrical conductivity, (d) thermopower, and (f) power factor for n-type PbTe at concentration $n=5\times10^{19}$ cm^{-3} using $E_{ac}=15$ eV and $E_{oc}=15$ eV. Theoretical values using temperature dependent m_d and E_g are shown as dashed lines and the experimental values are shown as black points from Ref. 20 and as gray points from Ref. 15.

mated. Over the entire 300–950 K temperature range the agreement for electrical conductivity with experiment is quite good, suggesting that $E_{ac}=15$ eV and $E_{oc}=15$ eV values of the deformation potential coupling constants describe well the scattering mechanisms in the $1-10\times10^{19}$ cm^{-3} concentration range. The thermopower is overestimated for both concentrations; as a consequence the power factor is also overestimated.

B. PbTe using *ab initio* electronic structure

In order to calculate the transport coefficients of n-type PbTe using *ab initio* density functional results one has to carry out summations over $\vec{k}$ and different bands. The carrier velocities were calculated using the momentum matrix elements. It was found that a very dense mesh of irreducible $\vec{k}$ points (more than 15 000) in the Brillouin zone has to be taken in order to have good convergence for the values of the transport coefficients. This will require a tremendous amount of computational time and computer resources in the case of complex LAST-m systems, but for PbTe such calculations are currently feasible. For the relaxation time the same expressions were used as in the nonparabolic Kane model, taking into account the temperature dependence of E_g and m_d.

The calculated values for the electrical conductivity and thermopower at $n=5\times10^{19}$ cm^{-3} are shown in Fig. 6. One expects that *ab initio* energy dispersion should give better agreement with experiment as compared to the Kane model. In contrast the agreement is not as good. The electrical conductivity is overestimated [Fig. 6(a)] and the thermopower is underestimated [Fig. 6(b)]. This is due to the fact that in *ab initio* calculations the temperature dependence of the density of states effective mass m_d cannot be incorporated in the calculation of chemical potential. For the same n, the *ab initio* results give a higher value of the chemical potential μ than that given by the Kane model. This results in an increase in the electrical conductivity and a decrease in the magnitude of the thermopower at a given temperature. To confirm that not incorporating the temperature dependence of m_d in theoretical calculations is the reason for disagreement between the *ab initio* results and experiment, we have calculated the transport coefficients in the Kane model using constant values for m_d in the expression for concentration n [Eq. (A16)] but temperature dependent m_d in the expressions of relaxation times. These results are shown in Figs. 6(a) and 6(b) as continuous lines, and they clearly show an overestimation of electrical conductivity and underestimation of thermopower. The zero temperature *ab initio* electronic structure calculations cannot correctly describe the finite temperature transport coefficients in PbTe when the band structure parameters such as E_g and m_d are strongly T dependent. The main problem is that the temperature dependence of the chemical potential is not correctly accounted for.

C. LAST-m using a modified Kane model

To calculate the transport properties of LAST-m systems, we make use of the *ab initio* band structure results to con-

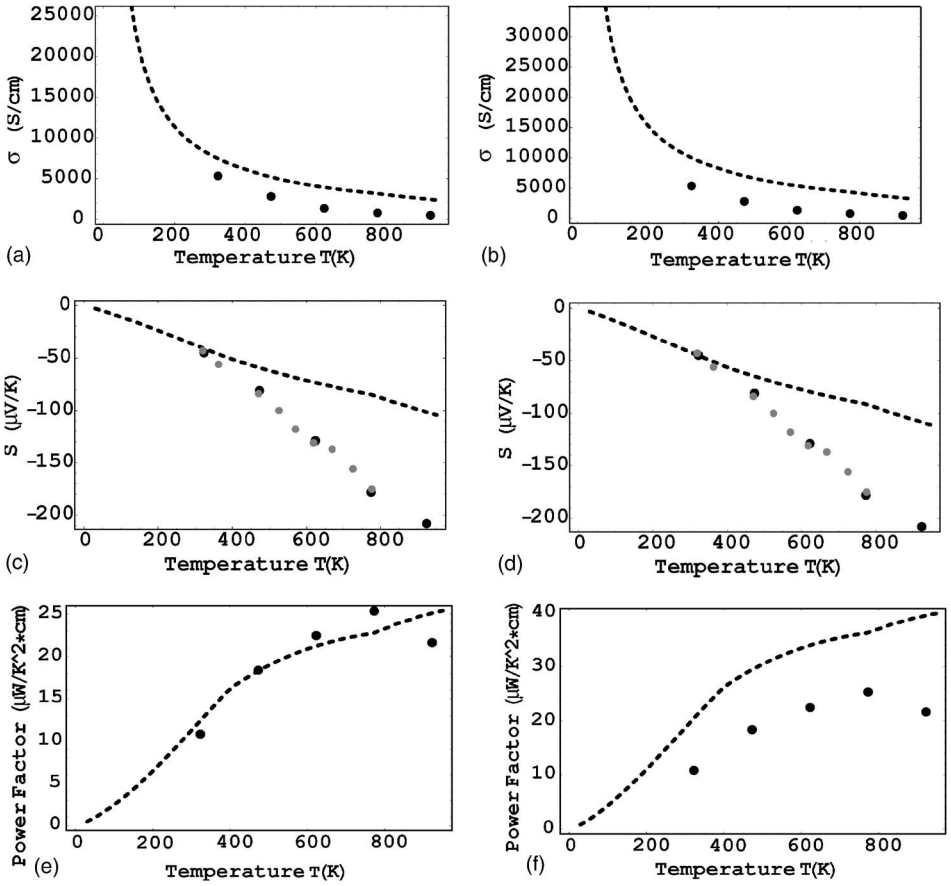

FIG. 3. Temperature dependence of (a) electrical conductivity, (c) thermopower, and (e) power factor for n-type PbTe at concentration $n=5\times10^{19}$ cm^{-3} obtained using $E_{ac}=15$ eV and $E_{oc}=26$ eV values of the deformation potential coupling constants. Temperature dependence of (b) electrical conductivity, (d) thermopower, and (f) power factor for n-type PbTe at concentration $n=5\times10^{19}$ cm^{-3} using coupling constant values $E_{ac}=15$ eV and $E_{oc}=15$ eV. Theoretical values obtained using constant m_d are shown as dashed lines. Experimental values are shown as black points from Ref. 20 and as gray points from Ref. 15.

struct an effective nonparabolic Kane model. Transport coefficient calculations were performed for the chain model of LAST-30 systems (Fig. 7) through a qualitative comparison between the band structure results of the chain model and bulk PbTe. The band structure of PbTe and the chain model in the simple cubic (sc) Brillouin zone[21] are given in Figs. 8(a) and 8(b). In the sc Brillouin zone of PbTe, the conduction band minimum and the valence band maximum occur at the Γ point, which is the same as the L point in the face-centered-cubic (fcc) Brillouin zone.[21] The lowest conduction band in the fcc Brillouin zone, which contributes to the transport, is onefold degenerate and the multiplicity of the L point is four, whereas in the sc Brillouin zone the lowest conduction band is fourfold degenerate and the multiplicity of the Γ point is one.

More specifically, the lowest conduction band in the sc Brillouin zone along the ΓX direction is fourfold degenerate, whereas in the ΓR direction the first conduction band is one-

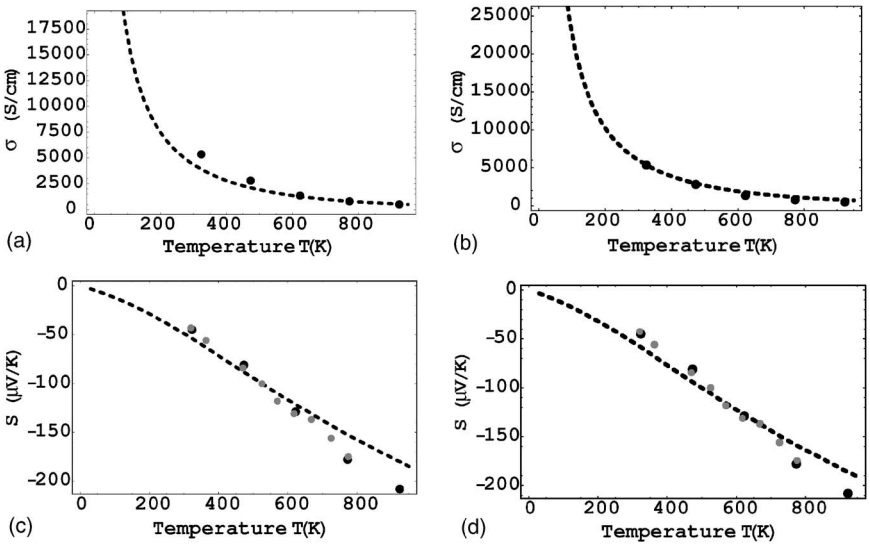

FIG. 4. Temperature dependence of (a) electrical conductivity, and (c) thermopower for n-type PbTe at concentration $n=5\times10^{19}$ cm^{-3} using $E_{ac}=15$ eV and $E_{oc}=26$ eV values of the deformation potential coupling constants. Temperature dependence of (b) electrical conductivity and (d) thermopower for n-type PbTe at concentration $n=5\times10^{19}$ cm^{-3} using coupling constant values $E_{ac}=15$ eV and $E_{oc}=15$ eV. Theoretical values obtained using temperature dependent E_g in the 0–950 K range are shown as dashed lines. Experimental values are shown as black points from Ref. 20 and as gray points from Ref. 15.

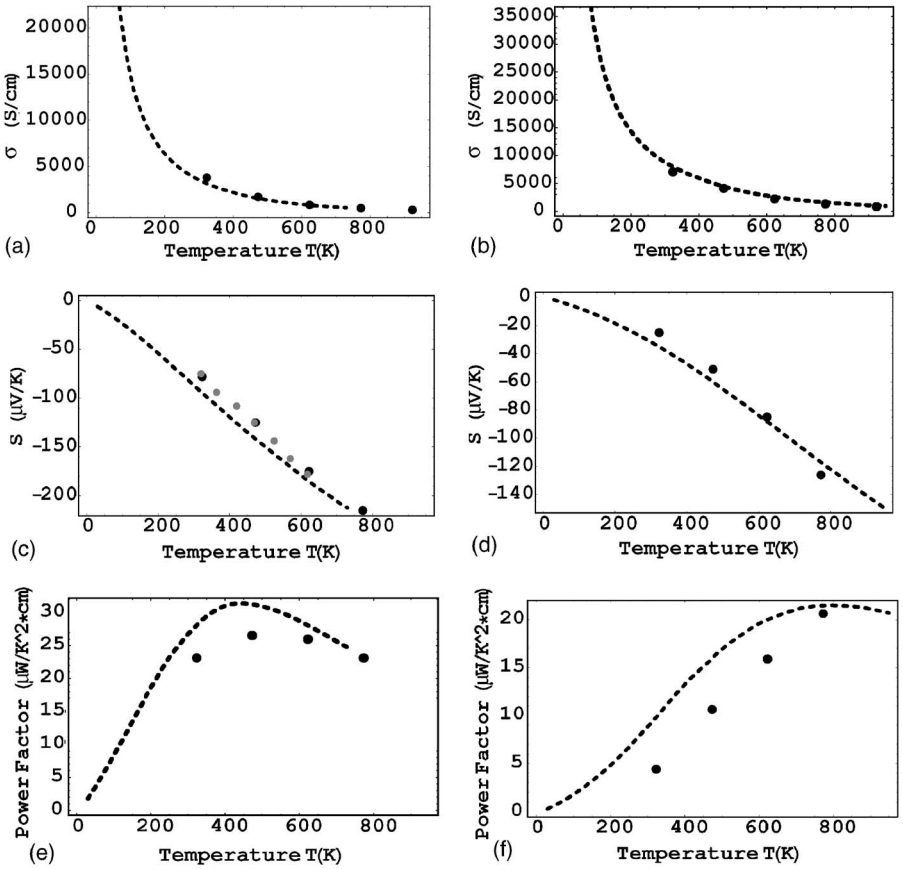

FIG. 5. Temperature dependence of (a) electrical conductivity, (c) thermopower, and (e) power factor for n-type PbTe at concentration $n=2.4\times10^{19}$ cm^{-3}. Temperature dependence of (b) electrical conductivity, (d) thermopower, and (f) power factor for n-type PbTe at concentration $n=10\times10^{19}$ cm^{-3}. Theoretical values obtained using temperature dependent E_g and m_d and using $E_{ac}=15$ eV and $E_{oc}=15$ eV values for the deformation potential coupling constants are shown as dashed lines. Experimental values are shown as black points from Ref. 20 and as gray points from Ref. 15.

fold degenerate and the second conduction band is threefold degenerate. For the chain model of LAST-30, we can clearly see a dramatic modification of the band structure near the bottom of the conduction band [Fig. 8(b)]. As was pointed out in Ref. 3, the presence of Sb in PbTe gives rise to resonant states in the conduction band. In that paper we had conjectured that the presence of resonant states may be the reason for large thermopower. As we see in Fig. 8(b), the Sb-induced resonant state lies at about 0.6 eV above the conduction band bottom. This state strongly hybridizes with one of the four PbTe conduction bands, giving a flatter energy dispersion for this band as compared to that of PbTe. Since the resonant state is 0.6 eV above the conduction band minimum, this state will not contribute directly to transport at carrier concentrations of interest. Therefore, to simulate the chain model for the lowest conduction band, we have taken a heavier density of states effective mass m_d^{chain}, whereas for the other three conduction bands we have used the same m_d as for PbTe. Although we recognize that this approach cannot quantitatively describe the chain model of LAST-30 systems since m_d for the other three conductions bands are not exactly the same as those of PbTe, this approach can qualitatively describe the transport properties in all LAST-m systems. This is a consequence of the electronic structure results, which show that several Ag-Sb microstructural arrangements have an enhanced conduction band density of states (heavier m_d) near the band bottom as compared to PbTe.[3]

We have considered two values for the effective mass m_d^{chain} of the lowest conduction band. One is $m_d^{chain}=1.5m_d$

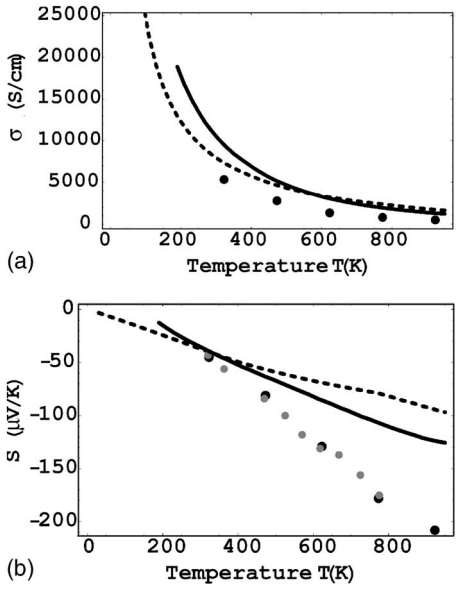

FIG. 6. Temperature dependence of (a) electrical conductivity and (b) thermopower for n-type PbTe at concentration $n=5\times10^{19}$ cm^{-3} and using $E_{ac}=15$ eV and $E_{oc}=15$ eV values of the deformation potential coupling constants. Theoretical values obtained using *ab initio* energy dispersion and temperature dependence of E_g and m_d are shown as dashed lines. Theoretical values obtained using nonparabolic Kane energy dispersion with constant m_d in the expression of n are shown as continuous lines. Experimental values are shown as black points from Ref. 20 and as gray points from Ref. 15.

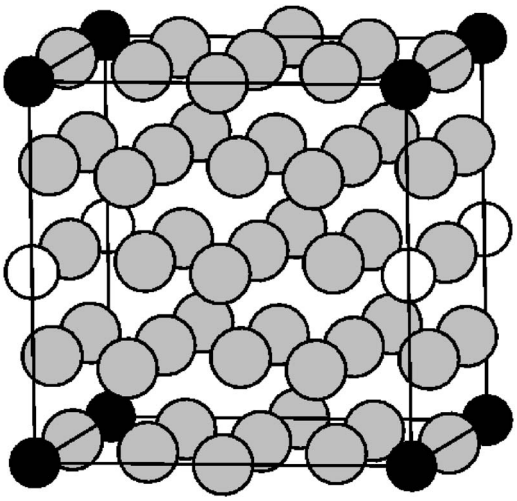

FIG. 7. Unit cell model for Ag-Sb chain parallel to the [001] direction in $AgSbPb_{30}Te_{32}$. For the reason of clarity we show only Pb fcc lattices with Pb in gray, Ag in white, and Sb in black colors.

and the other is $m_d^{chain}=2.5m_d$, where m_d is the density of states effective mass of PbTe, which was assumed to be temperature dependent. The results for concentration $n=5\times10^{19}$ cm^{-3} (using $E_{ac}=15$ eV and $E_{oc}=15$ eV values of the deformation potential coupling constants) are given in Fig. 9. The chain model for $m_d^{chain}=1.5m_d$ has a lower electrical conductivity and a higher thermopower compared to PbTe. As a result the power factor shows a small increase in the 0–500 K temperature range [Figs. 9(a), 9(c), and 9(e)]. Increasing the value of m_d^{chain} even further ($m_d^{chain}=2.5m_d$), the electrical conductivity of the chain model is further decreased, whereas the thermopower is increased. This gives an enhanced power factor in the 0–500 K temperature range [Figs. 9(b), 9(d), and 9(f)]. These qualitative transport calculations show that LAST-m systems in the 0–500 K temperature range have a small increase in the power factor compared to PbTe. The enhancement of the power factor increases with the increasing m_d^{chain} values.

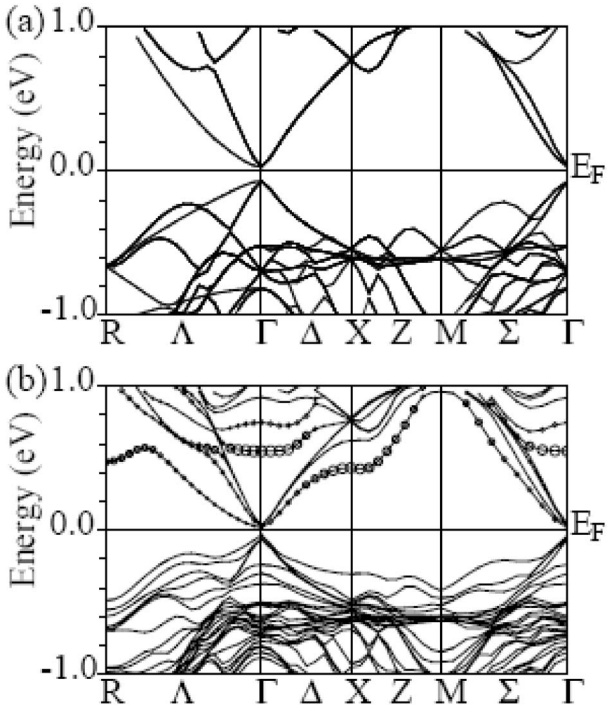

FIG. 8. (a) Band structure in simple cubic Brillouin zone of (a) bulk PbTe and (b) Ag-Sb chain model; orbital character of Sb p. The size of the circles is proportional to the strength of the orbital character.

We have calculated the transport coefficients for a higher concentration ($n=1\times10^{20}$ cm^{-3}) for $m_d^{chain}=2.5m_d$. These results are shown in Fig. 10. The power factor for this concentration shows an enhancement in the 0–700 K temperature range. This suggests that the temperature range for which the power factor of LAST-m systems shows an enhancement relative to PbTe increases with carrier concentration.

VII. SUMMARY

Transport calculations using the nonparabolic Kane model for energy dispersion in PbTe show that the temperature dependence of the density of states effective mass m_d is very important to correctly describe the temperature dependence of electrical conductivity and thermopower. Taking into account this temperature dependence and that of the energy band gap, we see that the electrical conductivity has a T^{-3} temperature dependence (in agreement with experiment).[11]

Calculations for PbTe using *ab initio* electronic structure results for the energy dispersion overestimate the electrical conductivity and underestimate the thermopower at a given temperature. This is a consequence of the fact that in *ab initio* electronic structure results, the temperature dependence of density of states cannot be taken into account in the calculation of the chemical potential. This increases the chemical potential values for a given n and temperature. This effect enhances the electrical conductivity and reduces the thermopower. Therefore, the zero temperature *ab initio* density functional theory (DFT) cannot describe correctly the transport properties in PbTe when m_d and E_g are known to depend strongly on T. This is also true for the LAST-m materials.

In the LAST-30 compound, the presence of Sb gives rise to resonant states in the conduction band, which lies ~0.6 eV above the conduction band bottom and as a result, does not directly contribute to the transport properties. However, it indirectly affects the transport by altering the dispersion of the conduction band states resulting from hybridization effects. The transport calculations for the chain model of LAST-30, taking into account the change in density of states, show a small enhancement of the power factor in the 0–500 K temperature range relative to PbTe. This enhancement increases with increasing m_d values. The temperature range for which this enhancement of the power factor is achieved increases with increasing n. These results show that the enhanced DOS of LAST-m systems near the band gap do not always increase the power factor compared to PbTe. The power factor values depend sensitively on m_d and n values. This may explain why it is very difficult to reproduce the

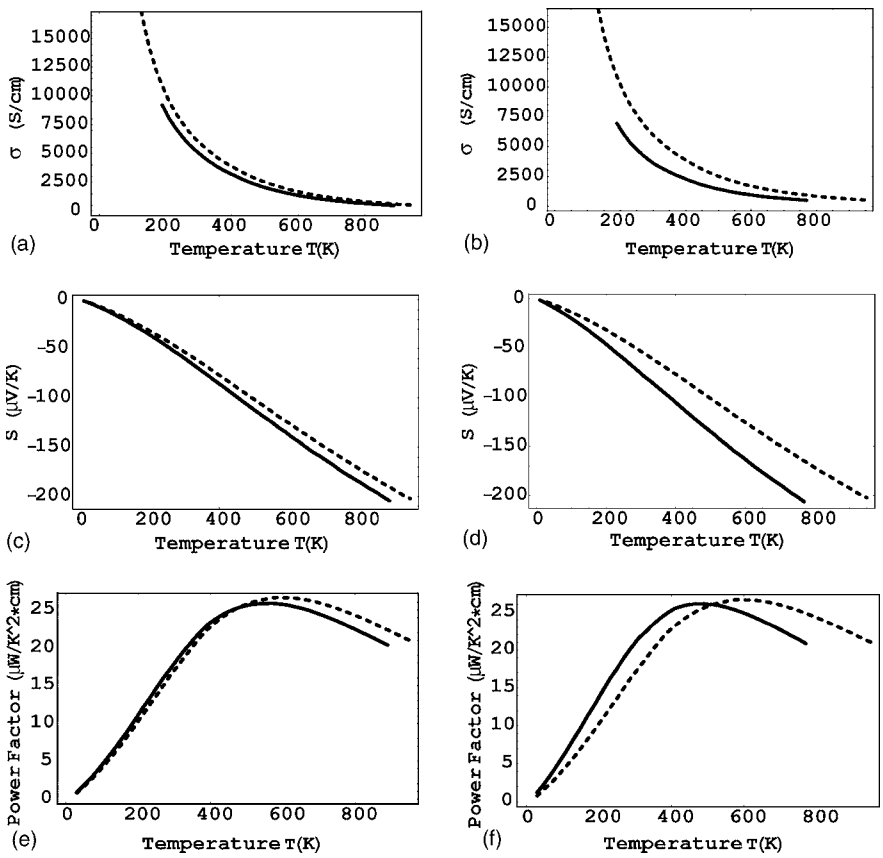

FIG. 9. Transport coefficients at concentration $n=5\times10^{19}$ cm^{-3} using temperature dependent E_g and m_d and $E_{ac}=15$ eV and $E_{oc}=15$ eV for the deformation potential coupling constants. Temperature dependence of (a) electrical conductivity, (c) thermopower, and (e) power factor for $m_d^{chain}=1.5m_d$. Temperature dependence of (b) electrical conductivity, (d) thermopower, and (f) power factor for $m_d^{chain}=2.5m_d$. Theoretical values for bulk PbTe are shown as dashed lines and for the chain model of LAST-30 as continuous lines.

large ZT values in the LAST-m systems.

Transport calculations reveal that the enhanced density of states (enhanced m_d) near the band gap of LAST-m systems as compared to that of PbTe seen in the electronic structure calculations can give rise to a small increase in the power factor. However this increase is not large enough to increase ZT by a factor of ~ 2 (as seen experimentally). Therefore, the reason LAST-m systems have better ZT compared to PbTe is perhaps due to a strong reduction in the lattice thermal conductivity due to the formation of microstructures (seen in electron microscopy).[2]

ACKNOWLEDGMENT

Financial support from the Office of Naval Research (Contract No. N00014-02-1-0867 MURI program) is gratefully acknowledged.

APPENDIX

The Kane model energy dispersion Eq. (6) contains two types of effective masses and in order to simplify the calculations, the following substitutions can be made:

$$k_t^2 = \frac{m_t}{m_d'} k_t'^2, \tag{A1}$$

$$k_l^2 = \frac{m_l}{m_d'} k_l'^2. \tag{A2}$$

where m_d' is related to density of states effective mass m_d by Eq. (A17). Using the new variables k_l' and k_t', Eq. (6) can be written as

$$\epsilon_{k'}\left(1+\frac{\epsilon_{k'}}{E_g}\right) = \frac{\hbar^2}{2m_d'}(2k_t'^2 + k_l'^2) \equiv \frac{\hbar^2}{2m_d'}k'^2. \tag{A3}$$

In terms of the new variable $\vec{k}'$ the expressions for $\overleftrightarrow{\sigma}$ and $\overleftrightarrow{S}$ are

$$\overleftrightarrow{\sigma} = \frac{e^2}{V}\sum_{\vec{k}'}\left(-\frac{\partial f_{\vec{k}'}}{\partial \epsilon_{\vec{k}'}}\right)\tau_{\vec{k}'}\vec{v}_{\vec{k}'}\vec{v}_{\vec{k}'}, \tag{A4}$$

$$\overleftrightarrow{S} = (\overleftrightarrow{\sigma})^{-1}\overleftrightarrow{A}, \tag{A5}$$

where $\overleftrightarrow{A}$ is given by

$$\overleftrightarrow{A} = \frac{e}{VT}\sum_{\vec{k}'}\left(-\frac{\partial f_{\vec{k}'}}{\partial \epsilon_{\vec{k}'}}\right)(\epsilon_{\vec{k}'}-\mu)\tau_{\vec{k}'}\vec{v}_{\vec{k}'}\vec{v}_{\vec{k}'}. \tag{A6}$$

Changing the sums into integrals, Eq. (A5) for thermopower becomes

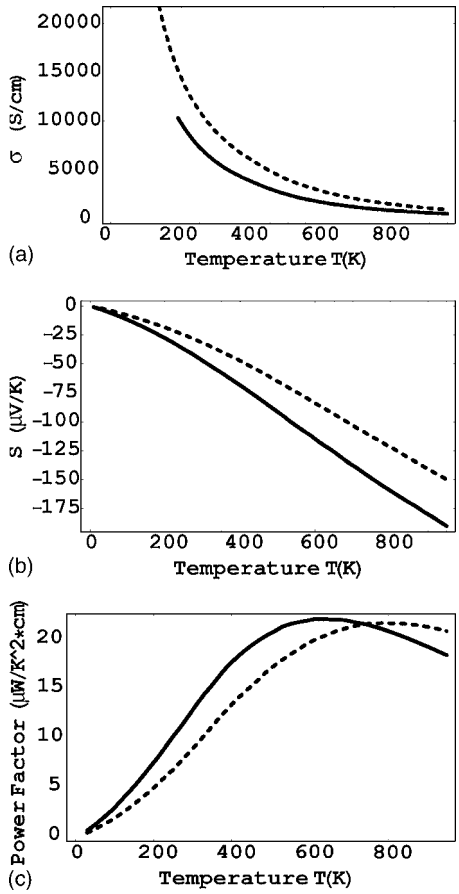

FIG. 10. Transport coefficients at concentration $n=1\times10^{20}$ cm^{-3} using temperature dependent E_g and m_d and $E_{ac}=15$ eV and $E_{oc}=15$ eV values of the deformation potential coupling constants. Temperature dependence of (a) electrical conductivity, (b) thermopower, and (c) power factor for $m_d^{chain}=2.5m_d$. Theoretical values for bulk PbTe are shown as dashed lines and for the chain model of LAST-30 as continuous lines.

$$\vec{\vec{S}}=\frac{1}{eT}\frac{\int_0^\infty\left(-\frac{\partial f_{\vec{k}'}}{\partial\epsilon_{\vec{k}'}}\right)(\epsilon_{\vec{k}'}-\mu)\tau_{\vec{k}'}\vec{v}_{\vec{k}'}\vec{v}_{\vec{k}'}d^3\vec{k}'}{\int_0^\infty\left(-\frac{\partial f_{\vec{k}'}}{\partial\epsilon_{\vec{k}'}}\right)\tau_{\vec{k}'}\vec{v}_{\vec{k}'}\vec{v}_{\vec{k}'}d^3\vec{k}'}. \tag{A7}$$

Using Eq. (A3), the infinitesimal unit volume in reciprocal space $d^3\vec{k}'$ can be expressed as

$$d^3\vec{k}'=4\pi k'^2dk'=4\pi\frac{2^{1/2}m_d'^{3/2}}{\hbar^3}\left[\epsilon\left(1+\frac{\epsilon}{E_g}\right)\right]^{1/2}\left(1+\frac{2\epsilon}{E_g}\right)d\epsilon, \tag{A8}$$

where we have dropped the suffix for the carrier energy $\epsilon_{\vec{k}'}$.

The carrier velocity is given by

$$\vec{v}_{\vec{k}'}=\frac{1}{\hbar}\frac{\partial\epsilon}{\partial\epsilon_{\vec{k}'}}=\frac{\hbar}{m_d'}\frac{\vec{k}'}{1+\frac{2\epsilon}{E_g}}. \tag{A9}$$

Using the above equation, the $\vec{v}^2_{\vec{k}'}$ term in the transport equations can be expressed as

$$v^2_{\vec{k}'}=\frac{2}{m_d'}\frac{\epsilon\left(1+\frac{\epsilon}{E_g}\right)}{\left(1+\frac{2\epsilon}{E_g}\right)^2}. \tag{A10}$$

Substituting Eqs. (A8) and (A10) into Eq. (A7) and using Eqs. (8) and (10), the thermopower along the x axis S_{xx} ($S_{xx}=S$) becomes

$$S_{xx}=\frac{1}{eT}\frac{\int_0^\infty\left(-\frac{\partial f}{\partial\epsilon}\right)(\epsilon-\mu)\left[\epsilon\left(1+\frac{\epsilon}{E_g}\right)\right]^{3/2}\left(1+\frac{2\epsilon}{E_g}\right)^{-1}\tau_\epsilon d\epsilon}{\int_0^\infty\left(-\frac{\partial f}{\partial\epsilon}\right)\left[\epsilon\left(1+\frac{\epsilon}{E_g}\right)\right]^{3/2}\left(1+\frac{2\epsilon}{E_g}\right)^{-1}\tau_\epsilon d\epsilon}, \tag{A11}$$

where the relaxation time τ_ϵ is assumed to depend only on energy. Since S depends on the ratio of the two integrals [Eq. (A7)] the spin and band degeneracy γ factors cancel out in Eqs. (A7) and (A11).

Taking into account the spin degeneracy and the band degeneracy γ, the expression for the electrical conductivity $\vec{\vec{\sigma}}$ can be rewritten as

$$\vec{\vec{\sigma}}=\frac{2\gamma e^2}{V}\sum_{\vec{k}'}\left(-\frac{\partial f_{\vec{k}'}}{\partial\epsilon_{\vec{k}'}}\right)\vec{v}_{\vec{k}'}\vec{v}_{\vec{k}'}\tau_{\vec{k}'}=\frac{2\gamma e^2}{V}\frac{V}{(2\pi)^3}\times\int_0^\infty\left(-\frac{\partial f_{\vec{k}'}}{\partial\epsilon_{\vec{k}'}}\right)\vec{v}_{\vec{k}'}\vec{v}_{\vec{k}'}\tau_{\vec{k}'}d^3\vec{k}', \tag{A12}$$

and using Eqs. (A8) and (A10), Tr $\vec{\vec{\sigma}}$ can be expressed as

$$\text{Tr }\sigma=2\gamma e^2\frac{(2m_d')^{1/2}}{\pi^2\hbar^3}\int_0^\infty\left(-\frac{\partial f}{\partial\epsilon}\right)\left[\epsilon\left(1+\frac{\epsilon}{E_g}\right)\right]^{3/2}\times\left(1+\frac{2\epsilon}{E_g}\right)^{-1}\tau_\epsilon d\epsilon. \tag{A13}$$

In order to compare the electrical conductivity with the measured experimental values along a specific crystallographic direction (i.e., x axis), the component σ_{xx} has to be calculated. σ_{xx} ($\sigma_{xx}=\sigma$) is given by

$$\sigma_{xx}=\frac{2}{3}\gamma e^2\frac{(2m_d')^{1/2}}{\pi^2\hbar^3}\int_0^\infty\left(-\frac{\partial f}{\partial\epsilon}\right)\left[\epsilon\left(1+\frac{\epsilon}{E_g}\right)\right]^{3/2}\times\left(1+\frac{2\epsilon}{E_g}\right)^{-1}\tau_\epsilon d\epsilon. \tag{A14}$$

The concentration of carriers n can be written as

$$n=\frac{2\gamma}{V}\sum_{\vec{k}'}f_{\vec{k}'}=\frac{2\gamma}{V}\frac{V}{(2\pi)^3}\int\frac{d^3\vec{k}'}{\exp\left(\frac{\epsilon_{\vec{k}'}-\mu}{K_BT}\right)+1}, \tag{A15}$$

and using Eq. (A8) the concentration n can be expressed as

$$n = \frac{2^{1/2}}{\pi^2\hbar^3}\gamma m_d'^{3/2}\int_0^\infty \frac{\left[\epsilon\left(1+\frac{\epsilon}{E_g}\right)\right]^{1/2}\left(1+\frac{2\epsilon}{E_g}\right)d\epsilon}{\exp\left(\frac{\epsilon-\mu}{K_BT}\right)+1}. \tag{A16}$$

The expression $\gamma m_d'^{3/2}$ is defined as

$$m_d^{3/2} = \gamma m_d'^{3/2}, \tag{A17}$$

where m_d is called density of states effective mass. The relation between the density of states effective mass and longitudinal and transverse effective masses can be deduced using the Eqs. (A1) and (A2), and the following equation:

$$d^3\vec{k} = d^3\vec{k}', \tag{A18}$$

which sets the equality between the infinitesimal volumes in reciprocal space. Then the density of states effective mass can be expressed as

$$m_d = \gamma^{2/3} m_d' = \gamma^{2/3}\left(m_l m_t^2\right)^{1/3}. \tag{A19}$$

[1] K. F. Hsu, S. Loo, F. Guo, W. Chen, J. S. Dyck, C. Uher, T. Hogan, E. K. Polychroniadis, and M. G. Kanatzidis, Science **303**, 818 (2004).
[2] E. Quarez, K. F. Hsu, R. Pcionek, N. Frangis, E. K. Polychroniadis, and M. G. Kanatzidis, J. Am. Chem. Soc. (to be published).
[3] D. Bilc, S. D. Mahanti, E. Quarez, K. F. Hsu, R. Pcionek, and M. G. Kanatzidis, Phys. Rev. Lett. **93**, 146403 (2004).
[4] L. D. Hicks and M. S. Dresselhaus, Phys. Rev. B **47**, 12727 (1993).
[5] T. C. Harman, P. J. Taylor, M. P. Walsh, and B. E. LaForge, Science **297**, 2229 (2002).
[6] L. D. Hicks, T. C. Harman, and M. S. Dresselhaus, Appl. Phys. Lett. **63**, 3230 (1993).
[7] R. Venkatasubramanian, E. Siivola, T. Colpitts, and B. O'Quinn, Nature (London) **413**, 597 (2001).
[8] G. D. Mahan and J. O. Sofo, Proc. Natl. Acad. Sci. U.S.A. **93**, 7436 (1996).
[9] M. G. Kanatzidis, Semicond. Semimetals **69**, 51 (2001).
[10] M. G. Kanatzidis, *Chemistry, Physics, and Material Science of Thermoelectric Materials: Beyond Bismuth Telluride* (Kluwer Academic, New York, 2003), p. 35.
[11] Yu. I. Ravich, B. A. Efimova, and I. A. Smirnov, *Semiconducting Lead Chalcogenides* (Plenum Press, New York, 1970), Vol. 5, p. 299.
[12] H. Yokoi, S. Takeyama, N. Miura, and G. Bauer, Phys. Rev. B **44**, 6519 (1991).
[13] Y. W. Tsang and M. L. Cohen, Phys. Rev. B **3**, 1254 (1971).
[14] Yu. I. Ravich, B. A. Efimova, and V. I. Tamarchenko, Phys. Status Solidi B **43**, 11 (1971).
[15] Yu. I. Ravich, B. A. Efimova, and V. I. Tamarchenko, Phys. Status Solidi B **43**, 453 (1971).
[16] D. M. Zayachuk, Semiconductors **31**, 173 (1997).
[17] D. M. Freik, L. I. Nykyruy, and V. M. Shperun, Semicond. Phys., Quantum Electron. Optoelectron. **5**, 362 (2002).
[18] J. M. Ziman, *Principles of The Theory of Solids* (Cambridge University Press, New York, 1964), p. 179.
[19] P. Blaha, K. Schwarz, and J. Luitz, *WIEN2K, An Augmented Plane Wave + Local Orbitals Program for Calculating Crystal Properties* (Karlheinz Schwarz, Technical Universitat Wien, Austria, 2001).
[20] B. A. Efimova, L. A. Kolomoets, Yu. I. Ravich, and T. S. Stavitskaya, Sov. Phys. Semicond. **4**, 1653 (1971).
[21] R. M. Martin, *Electronic Structure, Basic Theory and Practical Methods* (Cambridge University Press, Cambridge, MA, 2004), p. 84.